

1 ***Floodplains, Organic Carbon Residence Times, and Paleoclimate: Floodplain Dynamics Impart Biases***  
2 ***in the Biogeochemical Climate Record of Terrestrial Landscapes***

3

4 Fernandes, Anjali M.<sup>1</sup>, Hren, Michael T.<sup>2</sup>, Smith, Virginia B.<sup>3</sup>, Arvind Singh<sup>4</sup>, Terry Jr., Dennis O.<sup>5</sup>

5

6 <sup>1</sup>Department of Earth and Environmental Sciences, Denison University, 100 W College Street, Granville,  
7 Ohio, 43023

8 <sup>2</sup>Michael T. Hren, Department of Earth Sciences, University of Connecticut

9 <sup>3</sup>Virginia B. Smith, Department of Civil and Environmental Engineering, Villanova University,

10 Philadelphia

11 <sup>4</sup>Arvind Singh, Department of Civil, Environmental and Construction Engineering, University of Central

12 Florida

13 <sup>5</sup>Dennis O. Terry Jr., Department of Earth and Environmental Science, Temple University

14

15 Corresponding author: [fernandes@denison.edu](mailto:fernandes@denison.edu)

16

17 This is a non peer-reviewed pre-print submitted to EarthArXiv, and in review at Geophysical Research  
18 Letters.

19

20

21 ***Floodplains, Organic Carbon Residence Times, and Paleoclimate: Floodplain Dynamics Impart Biases***  
22 ***in the Biogeochemical Climate Record of Terrestrial Landscapes***

23  
24 Fernandes, Anjali M.<sup>1</sup>, Hren, Michael T.<sup>2</sup>, Smith, Virginia B.<sup>3</sup>, Arvind Singh<sup>4</sup>, Terry Jr., Dennis O.<sup>5</sup>

25

26 <sup>1</sup>Department of Earth and Environmental Sciences, Denison University, 100 W College Street, Granville,  
27 Ohio, 43023

28 <sup>2</sup>Michael T. Hren, Department of Earth Sciences, University of Connecticut

29 <sup>3</sup>Virginia B. Smith, Department of Civil and Environmental Engineering, Villanova University,  
30 Philadelphia

31 <sup>4</sup>Arvind Singh, Department of Civil, Environmental and Construction Engineering, University of Central  
32 Florida

33 <sup>5</sup>Dennis O. Terry Jr., Department of Earth and Environmental Science, Temple University

34

35 Corresponding author: [fernandesa@denison.edu](mailto:fernandesa@denison.edu)

36 **Plain language summary**

37

38 Along with the mineral sediment they transport (e.g., sand and mud), rivers also move organic carbon  
39 across continents and to oceans. Organic carbon particles can be stored in river sediment all along the  
40 river corridor, and then eventually remobilized. As a result, quantifying the time taken by organic carbon  
41 to move through the river network is challenging. In this work, we use experiments to explore how a  
42 changing climate might impact the rates at which carbon moves through rivers. We find that if a river  
43 begins to carry more water on average) than it used to, which is likely to happen as Earth's climate shifts

44 and intense rainfall events increase in frequency, the amount of time organic carbon spends on river  
45 floodplains will lengthen. On floodplains, organic carbon it is consumed by microbes and delivered to  
46 the atmosphere as CO<sub>2</sub>.

## 47 **Abstract**

48 Fluvial sediments encode physical and geochemical signatures of past climate, hydrology, carbon  
49 cycling and ecosystems. However, river floodplains can be both sources and sinks for organic carbon and  
50 paleoenvironmental reconstructions are often confounded by the complex dynamics of organic carbon  
51 residence, entrainment, and deposition in a fluvial system. We used physical experiments to explore how  
52 river kinematics impact the time over which organic carbon can accumulate on floodplain surfaces. We  
53 found that doubling the ratio of water to sediment flux caused the most stable parts of the floodplain to  
54 remain immobile for twice as long. In situ carbon accumulated on stable floodplains in this scenario, can  
55 therefore integrate significant amounts of local environmental information along with catchment-averaged  
56 information. Conversely, in situ organic carbon that accumulates on dynamic floodplains in systems with  
57 relatively high sediment fluxes predominantly records basin-averaged information but relatively small  
58 amounts of local information. Changes in river dynamics during past thermal events on Earth, linked to  
59 changes in the hydrological cycle and alterations in water and sediment fluxes, can be expected to alter  
60 the duration over which organic carbon can accumulate on Earth's river floodplains and therefore the  
61 spatial and temporal scales to which climate reconstructions apply.

## 62 **1. Introduction**

63 Rivers are gauges of environmental change, and their floodplains can serve as both sources and  
64 sinks for organic carbon. River channels erode, transport and deposit sediment as they build depositional  
65 landscapes, nourish ecological communities that rely on them, and fill terrestrial sedimentary basins.  
66 Organic carbon in alluvial sediment can provide an abundance of evidence regarding the hydroclimate

67 and ecological setting along river corridors and on floodplains in deep time (e.g. Chang et al. 2021,  
68 2023)). However, robust reconstructions of Earth's river landscapes and ecosystems hinge upon our  
69 ability to distinguish the potential spatial and temporal scales of integration of ecological information  
70 recovered from the deep time sedimentary record. Climate variability, and related changes in temperature  
71 and precipitation, can alter the dynamics of rivers and their floodplains by altering water and sediment  
72 fluxes. Terrestrial climate reconstructions rarely account for the impact of river dynamics on the recorded  
73 environmental information.

74 Particulate organic carbon (POC) preserved in fluvial deposits, e.g., molecular biomarkers, leaves  
75 or bulk carbon, can provide a quantitative record of past environments and climate variability. For  
76 example, plant derived organic carbon or molecular biomarkers encode signatures of past precipitation  
77 amounts (Diefendorf 2010), ecosystem (Diefendorf 2011), or atmospheric carbon dioxide  
78 (O'Leary 1981, Schubert and Jahren 2012). Further, molecular distributions can record atmospheric vapor  
79 pressure deficit (Eley and Hren, 2018) and stable isotopes of plant-derived molecular biomarkers (e.g. *n*-  
80 alkanes) can contain a time-integrated record of precipitation  $d^2H$  (e.g. Sachse et al., 2012; Wang et al.,  
81 2017). A quantitative approach to the processes of production, integration and storage over geologic time  
82 is crucial for reconstructing past environmental conditions from carbon stored in fluvial deposits.

83 Organic matter present in sedimentary deposits (Fig. 1a) can be (a) detrital in origin and carry  
84 catchment-integrated environmental information, or (b) deposited *in situ* from local vegetation and  
85 provide information about local environmental conditions. If catchment-integrated, environmental signals  
86 may be integrated over millions of years, and represent spatial scales associated with the size of the  
87 catchment; if local, they may be integrated over years (e.g., fossil leaf beds) to thousands of years, and  
88 represent much smaller spatial scales. Thus, the separation of local from catchment-integrated information  
89 has significant implications for the spatiotemporal scales over which paleoenvironmental reconstructions  
90 from biogeochemical proxies apply. By extension, this impacts the granularity with which climate  
91 perturbations with a range of temporal scales can be reconstructed (Fig. 1b). Parsing signals of local or  
92 catchment-integrated climate is possible with the depositional context provided by sedimentary facies.

93 Organic matter is most abundant in floodplain sediments and sampling floodplain deposits provides our  
94 best chance to reconstruct local environmental state; however, not all floodplains are created equal. The  
95 organic carbon in young (recently deposits) floodplain sediment surfaces will be predominantly detrital or  
96 catchment-integrated with carbon sourced from any or all parts of the upstream catchment area; mature  
97 floodplain surfaces (i.e. floodplain environments that are stable long enough to begin to form soils) will  
98 have accrued significantly more built-up *in situ* organic carbon containing a local environmental signal.  
99 Thus, floodplain age and spatial variability in floodplain ages can significantly impact the fidelity of  
100 terrestrial paleoclimate reconstructions.

101 Over centuries or millennia, an alluvial river landscape (Fig. 1a) may evolve to be broadly  
102 differentiated into three regions: (1) the river channel, where deposits primarily store organic carbon and  
103 mineral detritus mobilized from the entire catchment upstream, (2) the active (proximal) floodplain,  
104 where deposited detrital sediment composition is gradually altered by weathering and local organic  
105 carbon from plant detritus accumulates in soils, and (3) the stable (distal) floodplain, where soil formation  
106 and the build-up of local organic carbon from plant matter dominates.

107 A laterally migrating river incorporates floodplain sediment into the transport system by bank  
108 erosion and leaves sediment behind in bars (Fig. 1a), thereby replacing a local climatic signal with a  
109 spatio-temporally integrated one (Eke et al, 2014). Rivers in alluvial basins build topographic relief  
110 because of higher rates of sediment deposition close to the channel (Fig. 1a). When the height of the water  
111 surface in the channel above the distal floodplain approaches one channel depth, the resulting hydraulic  
112 instability can cause a channel avulsion (Davies-Vollum & Kraus, 2001; Heller & Paola, 1996; Mohrig et  
113 al., 2000; Slingerland & Smith, 2004). Flow finds a new path at a lower elevation on the floodplain,  
114 where it may re-occupy an older abandoned channel or form a new channel (Chamberlin & Hajek, 2015;  
115 Edmonds et al., 2016; Hajek & Edmonds, 2014). If the newly avulsed channel erodes floodplain  
116 sediment, the stored (local) signal will be replaced by a spatially- and temporally averaged signal in the  
117 carbon record.

118           Thus, if the rates of *in situ* organic debris accumulation remain equal, a river system that migrates  
119 rapidly and avulses frequently will primarily accumulate inherited, catchment-integrated environmental  
120 information in immature floodplains and the proportion of locally-sourced carbon stored will be small; a  
121 less dynamic system in which floodplains remain stable for longer periods of time will accumulate more  
122 *in situ* environmental information from local organic carbon, and the proportion of local carbon will be  
123 larger and overall age of the carbon pool younger. We therefore hypothesize that river dynamics,  
124 influenced by the ratio of water flux to sediment flux, impact (a) the residence time of *in situ* organic  
125 carbon in floodplains, and (b) the temporal and spatial integration of environmental information recovered  
126 from floodplain sediment.

127           Here, we use physical experiments of a distributive alluvial system to explore the role of channel  
128 and floodplain dynamics, influenced by differences in water and sediment flux, on the spatial variability  
129 in floodplain age and inferred variability in the recorded environmental information. In particular, we use  
130 an experimental distributive fan system to evaluate how differences in the ratio of water discharge to  
131 sediment discharge can impact: (1) landscape stability, and (2) spatial heterogeneity in floodplain age.  
132 Based on our findings, we draw inferences about carbon residence times and the biases in paleoclimate  
133 reconstructions from the biogeochemical proxy record.

134

## 135           **2. Experimental Conditions**

136           We used two physical experiments, performed at Tulane University (Straub & Wang, 2013; Y.  
137 Wang et al., 2011), to evaluate how the kinematics of the transport system influence floodplain stability.  
138 In these experiments, a fan delta evolved freely under two sets of steady boundary conditions. We used  
139 these data-sets to evaluate the influence of the ratio of water discharge to sediment discharge on  
140 floodplain stability, and therefore the potential heterogeneity in the recovered biomarker record.

141           The experiments were performed in an experimental basin that was 0.65 m deep, and measured  
142 4.2 m and 2.8 m in the downstream and cross-stream directions respectively (Straub & Wang, 2013; Y.  
143 Wang et al., 2011). A mixture of silica, crushed coal and water was released into the experimental basin at  
144 a constant rate and under the influence of gravity. The water in the mixture was dyed blue. In physical  
145 experiments such as these, unrealistic geometric scales (high ratios of particle size to flow depths, steep  
146 transport slopes, etc.) compared to natural systems are ignored as long as a range of transport styles, i.e.  
147 from bedload to suspended load, are observed (C. Paola et al., 2009). The sediment mixture, composed of  
148 a 3:7 volumetric ratio of crushed coal (S.G. = 1.3;  $D_{50} = 440\mu\text{m}$ ) and higher density silica (S.G. = 2.65;  
149  $D_{50} = 110\mu\text{m}$ ), allowed for a full spectrum of transport styles, from bedload to suspended load, in these  
150 experiments. Built by shallow channels with steep longitudinal profiles, the experimental deltas used  
151 herein do not display any influence from a backwater effect on channel dynamics e.g., (Fernandes et al.,  
152 2016; Ganti & Chadwick, 2016; Martin et al., 2018; Nittrouer et al., 2012; Chris Paola & Mohrig, 1996;  
153 Te Chow, 1959). The observed dynamics are therefore most relevant to fan deltas (e.g., (Nemec & Steel,  
154 1988) ) or distributive fluvial systems (e.g., (Hartley et al., 2010)).

155           Prior to the start of each experiment, sediment deposition built a prograding subaerial platform  
156 while base-level was maintained at a constant elevation; the experiment began once this initial platform  
157 was built. For the duration of each experiment, water supply, sediment supply and base-level rise rate  
158 pseudo-subsidence) were held constant (Table 1). The fixed rate at which accommodation was generated  
159 through base-level rise was matched against the fixed rate at which sediment was supplied such that the  
160 shoreline position did not change for the duration of each experiment. This stationarity precludes any  
161 potential influence that shoreline progradation or regression, equivalent to facies belt migration at the  
162 field-scale (Hickson et al., 2005), may have on the measured dynamics and organization in the transport  
163 system. In Experiments 1 and 2, the same base-level rise rate was used, but the ratio of water to sediment  
164 supplied to the basin in Experiment 2 was twice that of Experiment 1 (*Table 1*).

<i>Table 1: Boundary conditions associated with the physical experiments</i>		
Experiment	Experiment 1 (TDB-10-1)	Experiment 2 (TDB-11-1)
Water Flux : Sediment Flux Qw:Qs	1x 0.451 L/s : 0.011 L/s	2x 0.902 L/s : 0.011 L/s
Base-level rise rate	5mm/h	5mm / h
Duration of data-set used here	1000 min	1000 min

165 **3. Data and Methods**

166 We used sequential, orthorectified overhead images that represent 1000 timesteps (1000 minutes  
 167 of experimental time) from each experiment, we mapped the location and relative depth of flow through  
 168 time across the surface of each experiment. We applied two thresholds to the blue luminosity pixel values  
 169 in these overhead images, using a methodology implemented in a number of previous studies (e.g., Li et  
 170 al., 2016; Scheidt et al., 2016). The two thresholds were set and verified using visual inspection (Fig. 2),  
 171 and then used to separate dry portions of the experiment (without blue dye) from locations inundated by  
 172 shallow flow (small values of blue luminosity) and deeper, channelized flow (larger values of blue  
 173 luminosity).

174 We use deep, channelized flow as representative of river channels in field-scale fluvial systems;  
 175 shallow, sheet flow represents overbank flow in active floodplains; dry areas of the experimental surface  
 176 represent stable floodplain (Fig. 1a, 2). Channelized flow and sheet flow in similar fan delta experiments  
 177 have been shown to be associated with periods of sediment erosion and storage, respectively (Sheets et  
 178 al., 2002). During periods of sediment erosion or downstream flushing, the area of the surface that is  
 179 occupied by deeper flow in channels increases. Over time, sediment is flushed through the system and  
 180 deposited at the downstream termini of channels, reducing the longitudinal channel gradient (Kim et al.,

181 2014). The resulting decrease in sediment transport capacity causes channel filling, lateral flow expansion  
182 and widespread inundation by sheet flow. Inundation by sheet flow creates widespread deposition and a  
183 steepening of the longitudinal gradient.

184 In each experiment, we used one cross-stream transect at which cumulative deposition between  
185 the inlet and the transect accounted for approximately 60% of the sediment mass (Straub & Wang, 2013).  
186 At each pixel, we created a time-series to identify the presence of dry floodplain, channelized flow or  
187 sheet flow at each pixel along the transect (Fig. 2). Next, we generated distributions to quantify the  
188 fraction of the chosen transect that was occupied by each landscape state at each time-step (Fig. 3, a b).  
189 We then quantified the temporal persistence of each landscape state, i.e., floodplain (Fig. 3c, d), sheet  
190 flow (Fig. 3e, f), and channelized flow (Fig.3g, h). For example, when a pixel transitioned from wet  
191 (channelized flow or sheet flow) to dry floodplain, we counted the number of time-steps (experiment  
192 minutes) for which it remained dry before converting back to a wet surface.

193 Finally, we generated a comparative assessment of the impact of a difference in the ratio of water  
194 to sediment flux on the heterogeneity in floodplain age across a landscape transect at a given time (Fig.  
195 4). To assess the potential variability encountered along the geomorphic surface at any given time, such as  
196 at 1000 minutes (Fig. 4 a, b), we used the calculated ages of floodplain surfaces for all 1000 time steps  
197 (Fig. 4 c, d) to generate cumulative frequency distributions of instantaneous floodplain ages for each  
198 time-step and all time-steps together (Fig. 4 e, f), and exceedance probabilities for the floodplain surface  
199 ages encountered on a geomorphic surface at any time (Fig. 4, g, h).

## 200 **Results**

201 The fraction of the selected transects occupied by floodplain, sheet flow and channelized flow  
202 (Fig.3 a, b) are not significantly different between experiments. As indicated by the 25th, 50th and 75th  
203 percentiles, denoted hereafter by p25, p50 and p75 respectively, floodplains occupied a slightly larger  
204 fraction of the transect in Experiment 1 (p25 = 0.4, p50 = 0.5, p75 = 0.6) than in Experiment 2 (p25 =

205 0.33, p50 = 0.42, p75 = 0.52; Fig. 3 a, b). Sheet flow generally covered a larger fraction of the transect  
206 than channelized flow in both experiments; sheet flow occupied a smaller fraction of the transect in  
207 Experiment 1 (p25 = 0.28, p50 = 0.35, p75 = 0.43) than in Experiment 2 (p25 = 0.3, p50 = 0.4, p75 =  
208 0.5), whereas channelized flow generally occupied a similar fraction in Experiment 1 (p25 = 0.08, p50  
209 = 0.14, p75 = 0.20) and Experiment 2 (p25 = 0.13, p50 = 0.15 p75 = 0.2).

210           There were significant differences in the persistence of floodplains, sheet flow and channelized  
211 flow in the two experiments; all categories were generally more persistent in Experiment 2. Notably,  
212 doubling the ratio of water flux to sediment flux resulted in floodplain stability timescales (Fig. 3 c, d)  
213 that were roughly twice in Experiment 2 (p50 = 10 minutes, p95 = 96 minutes) than in Experiment 1 (p50  
214 = 5 minutes, p95 = 48 minutes). Sheet flow stability timescales in Experiment 1 (p50 = 5 minutes, p95 =  
215 18 minutes) were smaller than in Experiment 2 (p50 = 6 minutes, p95 = 33 minutes); similarly, stability  
216 timescales of channelized flow, i.e., the length of time for which channelized flow remained in place, in  
217 Experiment 1 (p50 = 4 minutes, p95 = 14 minutes) were smaller than in Experiment 2 (p50 = 6 minutes,  
218 p95 = 25 minutes). The number of measurements “n” in Figures 4 c - h, hold information about the  
219 fraction of the transect occupied by floodplain, sheet flow and channelized flow, as well as the mobility of  
220 each category; however, since the fraction of the transects occupied by each category were not  
221 significantly different between experiments, lower “n” values signify fewer measurements and therefore  
222 greater stability.

223           A visual assessment of Figure 4 a- d suggests that while floodplain extent, lateral continuity and  
224 frequency of occurrence in time are greater in Experiment 1, floodplain surfaces are generally young.  
225 This is internally consistent with the number of measurements (n = 13,126) in Figures 3c and 3d, as well  
226 as the smaller flow stability time-scales in Figures 3e and 3g. Conversely, floodplain surfaces tend to be  
227 spaced farther apart in time, are less continuous laterally and can be significantly older in Experiment 2;  
228 this assessment is supported by the smaller number of measurements in Figure 3d, and the larger flow  
229 stability timescales in Figures 3f and 3h. Importantly, these results of instantaneous floodplain ages on

230 geomorphic surfaces, quantified in Figures 4e & 4f, highlight that higher ratios of water to sediment  
231 fluxes in Experiment 2 generate floodplains ages (p50 = 20 minutes, p95= 100 minutes) that are generally  
232 twice that in Experiment 1 (p50 = 40 minutes, p95 = 100 minutes).

233 The exceedance probability calculations of floodplain age show power laws with higher slopes in  
234 Experiment 1 than in Experiment 2 (Fig. 4, g & h); the exceedance probability of encountering a  
235 floodplain surface with an age of 100 minutes is an order of magnitude higher in Experiment 2 than  
236 Experiment 1.

237

## 238 **Discussion**

239 Our results indicate that the morphodynamics of alluvial rivers, a function of sediment and water  
240 supply, can significantly impact the residence times of particulate organic carbon in Earth's floodplains  
241 and bias reconstructions of paleoclimate and paleotopography (Chang et al., 2023; Feakins et al., 2012;  
242 Hren et al., 2010; Hren & Ouimet, 2021; Pagani et al., 2006; Tipple et al., n.d.). Furthermore, although we  
243 specifically evaluate climate proxies tied to organic carbon in floodplains, our findings are relevant to any  
244 terrestrial climate proxies connected to timescales of floodplain stability (e.g., soil carbonates,  
245 geochemical climofunctions, etc.).

246 Comparing results from these experiments, we see that reduced relative sediment loads in  
247 Experiment 2, i.e., larger ratios of water flux to sediment flux ( $Q_w:Q_s$ ), decreased the lateral mobility of  
248 flow. Associated floodplain surfaces showed significantly more spatial variability in surface age and the  
249 oldest floodplain surfaces remained stable for twice as long relative to the oldest floodplain surfaces in  
250 Experiment 1. We can infer that organic carbon recovered from floodplains with greater stability are more  
251 likely to deliver paleoclimate reconstructions with temporal and spatial granularity that is commensurate  
252 with an *in situ*, unmixed environmental signal. However, the characteristic timescale associated with a  
253 significant build-up of local particulate organic carbon debris, a function of local hydroclimate, must be  
254 accounted for. For instance, an alluvial system in which the exceedance probability of floodplain age is

255 twice that of the characteristic timescale required to generate a clear *in situ* environmental signal may be  
256 expected to produce a record of local paleoenvironmental states at higher spatial and temporal resolution  
257 than one in which the two timescales are comparable.

258 Biomarkers recovered from channel deposits or young floodplain surfaces, on the other hand, can  
259 be expected to provide non-local or catchment-integrated estimate of hydroclimate with far less spatio-  
260 temporal granularity. Dynamic floodplain surfaces with greater spatial homogeneity in age, associated  
261 with alluvial systems in which smaller ratios of water to sediment flux, like Experiment 1, are more likely  
262 to be biased towards storing a catchment integrated record of paleoclimate. The spatial footprint of  
263 environmental reconstructions from channel deposits, or young floodplains, would likely scale with the  
264 size of the catchment. The temporal footprint would be dictated by the median age of carbon exported  
265 from the catchment.

266 Modern rivers display a latitudinal gradient in the ages of exported carbon (Eglinton et al., 2021)  
267 while high latitude rivers transport carbon with the greatest range in ages and largest ages. Climate  
268 models forecast an invigoration of the Earth's hydrological cycle as the planet warms; changing  
269 precipitation patterns that result are likely to drive changes in the ratios of water flux to sediment flux  
270 through rivers. In rivers that are allowed to migrate laterally, changes in lateral migration rates should be  
271 expected to produce differences in the range in the age of particulate organic carbon transported by rivers.  
272 Similarly, changes in river dynamics during thermal events in Earth's past, linked to changes in the  
273 hydrological cycle and alterations in water and sediment fluxes, should be expected to have altered carbon  
274 residence times in Earth's river systems. These alterations, and associated biases in terrestrial climate  
275 reconstructions, must be accounted for when reconstructing environmental conditions from particulate  
276 organic carbon preserved in floodplains. It is therefore essential to integrate biogeochemical proxy  
277 reconstructions with qualitative and quantitative information about sedimentary processes (e.g. floodplain  
278 stability and weathering, channel mobility, estimates of water and sediment fluxes, etc.), to assess the  
279 spatial and temporal scales to which paleoclimate reconstructions may apply.

280

281 **Conclusions**

282 We used physical experiments to investigate how river kinematics impact the duration over which  
283 organic carbon can accumulate on floodplain surfaces. Our findings indicate that doubling the ratio of  
284 water to sediment flux can cause the most stable parts of the floodplain to remain immobile for twice as  
285 long. Under such conditions, carbon accumulated on stable floodplains can integrate substantial amounts  
286 of local environmental information in addition to catchment-averaged data. Conversely, in more dynamic  
287 floodplains characterized by relatively high sediment fluxes, the in situ organic carbon predominantly  
288 records basin-wide environmental information with a comparatively minor contribution of local data.

289 Fluvial sediments can record the physical and geochemical signatures of past climates, hydrology,  
290 carbon cycling, and ecosystems. However, river floodplains function as both sources and sinks for  
291 organic carbon, complicating paleoenvironmental reconstructions due to the intricate dynamics of organic  
292 carbon residence, mobilization, and deposition within a fluvial system. Changes in river dynamics during  
293 past thermal events, which are linked to variations in the hydrological cycle and fluctuations in water and  
294 sediment fluxes, are expected to alter the duration over which organic carbon can accumulate on Earth's  
295 river floodplains. Consequently, these changes influence the spatial and temporal averaging of climatic  
296 information recovered from organic carbon. Our results indicate that reconstructions of ancient terrestrial  
297 climate must take into account the dynamics of the transport systems, and the stratigraphic fingerprints of  
298 these dynamics while assigning temporal and spatial scales to which these reconstructions apply.

299

300 **Acknowledgements**

301 This work was supported by funding from the National Science Foundation grants EAR-2023710 and  
302 EAR-2029803. The authors thank the Tulane Sediment Dynamics and Stratigraphy group and the  
303 Sediment Experimentalists Network for the collection and archival of experimental data.

304 **References cited**

- 305 Chamberlin, E. P., & Hajek, E. A. (2015). Interpreting paleo-avulsion dynamics from multistory sand  
306 bodies. *Journal of Sedimentary Research*
- 307 Chang, Q., Hren, M. T., Lai, L. S.-H., Dorsey, R. J., & Byrne, T. B. (2023). Rapid topographic growth of  
308 the Taiwan orogen since ~1.3-1.5 Ma. *Science Advances*, 9(25), eade6415.
- 309 Davies-Vollum, K. S., & Kraus, M. J. (2001). A relationship between alluvial backswamps and avulsion  
310 cycles: an example from the Willwood Formation of the Bighorn Basin, Wyoming. *Sedimentary*  
311 *Geology*.
- 312 Diefendorf, A. F., Mueller, K. E., Wing, S. L., Koch, P. L., & Freeman, K. H. (2010). Global patterns in  
313 leaf 13C discrimination and implications for studies of past and future climate. *Proceedings of the*  
314 *National Academy of Sciences of the United States of America*, 107(13), 5738–5743.
- 315 Edmonds, D. A., Hajek, E. A., Downton, N., & Bryk, A. B. (2016). Avulsion flow-path selection on  
316 rivers in foreland basins. *Geology*, 44(9), 695–698.
- 317 Eke, E., Parker, G., and Shimizu, Y., 2014, Numerical modeling of erosional and depositional bank  
318 processes in migrating river bends with self-formed width: Morphodynamics of bar push and bank  
319 pull: *Journal of Geophysical Research. Earth surface*, v. 119, p. 1455–1483.
- 320 Eley, Y. L., & Hren, M. T. (2018). Reconstructing vapor pressure deficit from leaf wax lipid molecular  
321 distributions. *Scientific Reports*, 8(1), 3967.
- 322 Feakins, S. J., Warny, S., & Lee, J.-E. (2012). Hydrologic cycling over Antarctica during the middle  
323 Miocene warming. *Nature Geoscience*, 5(8), 557–560.
- 324 Fernandes, A. M., Törnqvist, T. E., & Straub, K. M. (2016). Connecting the backwater hydraulics of  
325 coastal rivers to fluvio-deltaic sedimentology and stratigraphy.
- 326 Ganti, V., & Chadwick, A. J. (2016). Avulsion cycles and their stratigraphic signature on an experimental  
327 backwater-controlled delta. *Journal of Geophysical Research – Earth Surface*
- 328 Hajek, E. A., & Edmonds, D. A. (2014). Is river avulsion style controlled by floodplain

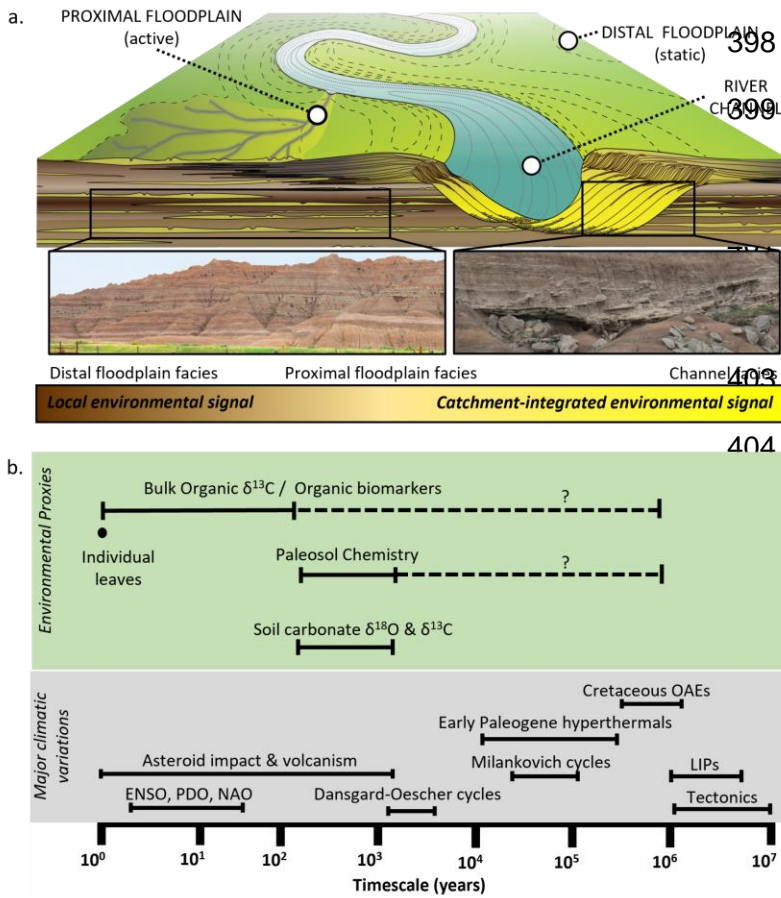
- 329 morphodynamics? *Geology*.
- 330 Hartley, A. J., Weissmann, G. S., Nichols, G. J., & Warwick, G. L. (2010). Large Distributive Fluvial  
331 Systems: Characteristics, Distribution, and Controls on Development. *Journal of Sedimentary*  
332 *Research*, 80(2), 167–183.
- 333 Heller, P. L., & Paola, C. (1996). Downstream changes in alluvial architecture; an exploration of controls  
334 on channel-stacking patterns. *Journal of Sedimentary Research*
- 335 Hickson, T. A., Sheets, B. A., Paola, C., & Kelberer, M. (2005). Experimental Test of Tectonic Controls  
336 on Three-Dimensional Alluvial Facies Architecture. *Journal of Sedimentary Research*, 75(4), 710–  
337 722.
- 338 Holloway, P. J. (1969). The effects of superficial wax on leaf wettability. *The Annals of Applied Biology*,  
339 63(1), 145–153.
- 340 Hren, M. T., & Ouimet, W. (2021). Organic Molecular Paleohypsometry: A New Approach to  
341 Quantifying Paleotopography and Paleorelief. *Frontiers of Earth Science*  
342 doi:/10.3389/feart.2021.665324
- 343 Hren, M. T., Pagani, M., Erwin, D. M., & Brandon, M. (2010). Biomarker reconstruction of the early  
344 Eocene paleotopography and paleoclimate of the northern Sierra Nevada. *Geology*, 38(1), 7–10.
- 345 Kim, W., Petter, A., Straub, K., & Mohrig, D. (2014). Investigating the autogenic process response to  
346 allogenic forcing: experimental geomorphology and stratigraphy. In A. W. Martinius, R. Ravnås, J.  
347 A. Howell, R. J. Steel, & J. P. Wonham (Eds.), *From Depositional Systems to Sedimentary*  
348 *Successions on the Norwegian Continental Margin* (Vol. 64, pp. 127–138). Chichester, UK: John  
349 Wiley & Sons, Ltd.
- 350 Li, Q., Yu, L., & Straub, K. M. (2016). Storage thresholds for relative sea-level signals in the stratigraphic  
351 record. *Geology*.
- 352 Martin, J., Fernandes, A. M., Pickering, J., Howes, N., Mann, S., & McNeil, K. (2018). The  
353 Stratigraphically Preserved Signature of Persistent Backwater Dynamics in a Large Paleodelta  
354 System: The Mungaroo Formation, Northwest Shelf, Australia. *Journal of Sedimentary Research*,

- 355 88(7), 850–872.
- 356 Mohrig, D., Heller, P. L., Paola, C., & Lyons, W. J. (2000). Interpreting avulsion process from ancient  
357 alluvial sequences: Guadalupe-Matarranya system (northern Spain) and Wasatch Formation (western  
358 Colorado). *GSA Bulletin*, 112(12), 1787–1803.
- 359 Neinhuis, C., & Barthlott, W. (1997). Characterization and Distribution of Water-repellent, Self-cleaning  
360 Plant Surfaces. *Annals of Botany*, 79(6), 667–677.
- 361 Nemec, W., & Steel, R. J. (1988). What is a fan delta and how do we recognize it. *Fan Deltas:  
362 Sedimentology and Tectonic Settings*, 3(13), 231–248.
- 363 Nittrouer, J. A., Shaw, J., Lamb, M. P., & Mohrig, D. (2012). Spatial and temporal trends for water-flow  
364 velocity and bed-material sediment transport in the lower Mississippi River. *Bulletin*. Retrieved  
365 from <https://pubs.geoscienceworld.org/gsa/gsabulletin/article-abstract/124/3-4/400/125770>
- 366 Pagani, M., Pedentchouk, N., Huber, M., Sluijs, A., Schouten, S., Brinkhuis, H., et al. (2006). Arctic  
367 hydrology during global warming at the Palaeocene/Eocene thermal maximum. *Nature*, 442(7103),  
368 671–675.
- 369 Paola, C., & Mohrig, D. (1996). Palaeohydraulics revisited: palaeoslope estimation in coarse-grained  
370 braided rivers. *Basin Research*, 8(3), 243–254.
- 371 Paola, C., Straub, K., Mohrig, D., & Reinhardt, L. (2009). The “unreasonable effectiveness” of  
372 stratigraphic and geomorphic experiments. *Earth-Science Reviews*.
- 373 Sachse, D., Billault, I., Bowen, G. J., Chikaraishi, Y., Dawson, T. E., Feakins, S. J., et al. (2012).  
374 Molecular Paleohydrology: Interpreting the Hydrogen-Isotopic Composition of Lipid Biomarkers  
375 from Photosynthesizing Organisms. <https://doi.org/10.1146/annurev-earth-042711-105535>
- 376 Scheidt, C., Fernandes, A. M., & Paola, C. (2016). Quantifying natural delta variability using a multiple-  
377 point geostatistics prior uncertainty model. *Journal of Geophysical Research*.
- 378 Sheets, B. A., Hickson, T. A., & Paola, C. (2002). Assembling the stratigraphic record: depositional  
379 patterns and time-scales in an experimental alluvial basin. *Basin Research*, 14(3), 287–301.
- 380 Slingerland, R., & Smith, N. D. (2004). River Avulsions And Their Deposits. *Annual Review of Earth*

- 381           and *Planetary Sciences*, 32(1), 257–285.
- 382   Straub, K. M., & Wang, Y. (2013). Influence of water and sediment supply on the long-term evolution of  
383           alluvial fans and deltas: Statistical characterization of basin-filling sedimentation patterns. *Journal of*  
384           *Geophysical Research. Earth Surface*, 118(3), 1602–1616.
- 385   Te Chow, V. (1959). *Open-channel hydraulics* (Vol. 1). McGraw-Hill New York.
- 386   Tipple, B. J., Meyers, S. R., & Pagani, M. (n.d.). Carbon isotope ratio of Cenozoic CO<sub>2</sub>: A comparative  
387           evaluation of available geochemical proxies. *Paleoceanography*.  
388           <https://doi.org/10.1029/2009PA001851>
- 389   Wang, C., Eley, Y., Oakes, A., & Hren, M. (2017). Hydrogen isotope and molecular alteration of n-  
390           alkanes during heating in open and closed systems. *Organic Geochemistry*, 112, 47–58.
- 391   Wang, Y., Straub, K. M., & Hajek, E. A. (2011). Scale-dependent compensational stacking: An estimate  
392           of autogenic time scales in channelized sedimentary deposits. *Geology*, 39(9), 811–814.
- 393   Yang, H., Liu, W., Leng, Q., Hren, M. T., & Pagani, M. (2011). Variation in n-alkane  $\delta$ D values from  
394           terrestrial plants at high latitude: Implications for paleoclimate reconstruction. *Organic*  
395           *Geochemistry*, 42(3), 283–288.

396

397



398 **Figure 1: (a)** An illustration showing  
 399 **sedimentary facies that provide**  
 400 **environmental context for the spatial**  
 401 **and temporal scales of integration**  
 402 **associated with the biogeochemical**  
 403 **climate proxies they hold. (b)**

404 **Representative time scales of major**  
 405 **modern climatic variations, and past**  
 406 **geologic events are compared to the**  
 407 **estimated time scales of integration**  
 408 **associated with different climate**  
 409 **proxies. Abbreviations: ENSO = El**  
 410 **Niño Southern Oscillation; PDO =**  
 411 **Pacific Decadal Oscillation; NAO =**

412 **North Atlantic Oscillation; OAEs = ocean anoxia events; LIPs = large igneous provinces. Solid range**  
 413 **bars correlate with assumptions of in situ information whereas dashed bars correlate with the potential**  
 414 **temporal scales of integration when the environmental signal is catchment integrated.**

415

416

417

418

419

420

421

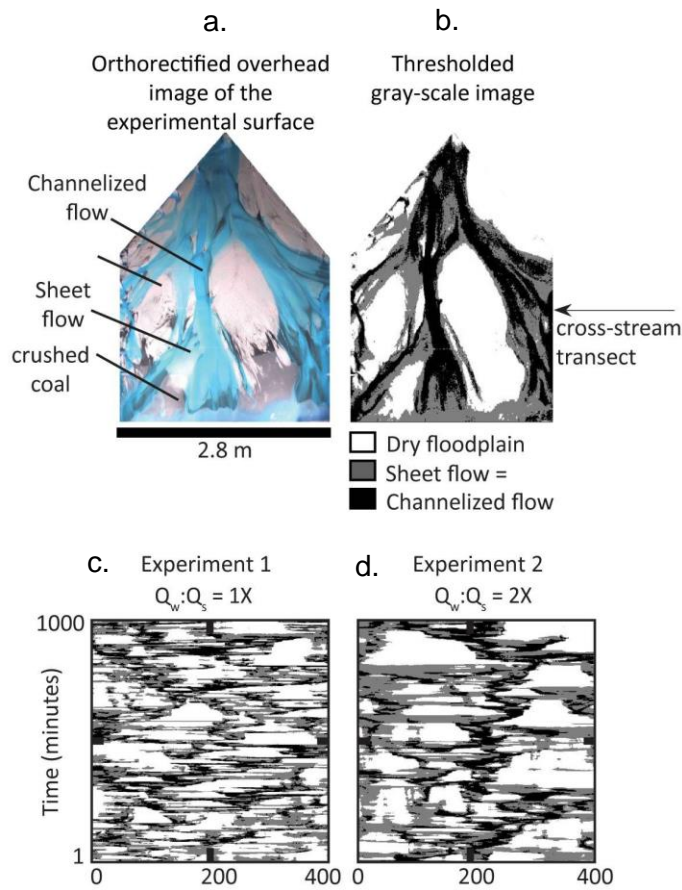


**Figure 2: Methodology applied to 1000 sequential orthorectified images from each experiment. (a) Orthorectified overhead full-color RGB images. (b) Thresholded gray-scale images where white pixels represent dry floodplain, grey pixels represent shallow sheet flow, and black pixels represent deep, channelized flow. Time-space matrices of stacked, thresholded pixel values at a cross stream transect from (c) Experiment 1, and (d) Experiment 2.**

435

436

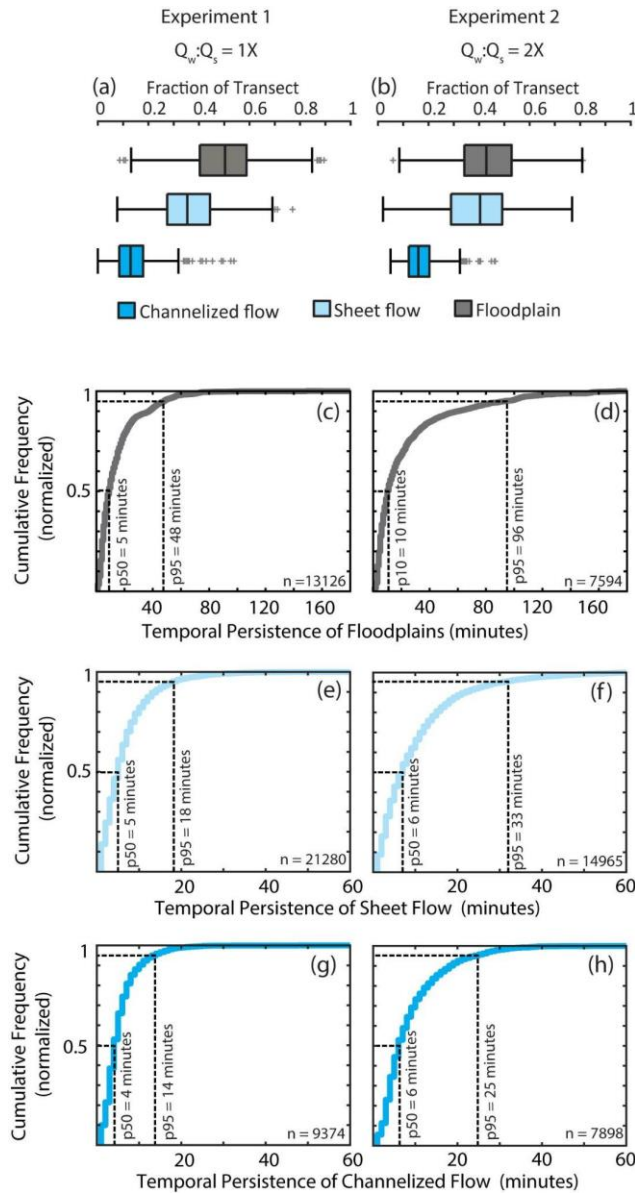


**Figure 3: Box and whisker plots showing the distribution in the fraction of the transect covered by floodplain, sheet flow and channelized flow at all 1000 time-steps in Experiment 1 (a) and Experiment 2 (b). The vertical bar at the center of the box represents the 50th percentile of values, the upper and lower bounds on the boxes represent the 25th and 75th percentiles respectively, and the upper and lower bounds on the whiskers represent the 10th and 90th percentile respectively. Normalized cumulative frequencies quantify temporal persistence of (c), (d) stable floodplain, (e), (f) sheet flow and (g), (h) channelized flow in Experiment 1 (left) and Experiment 2 (right) respectively.**

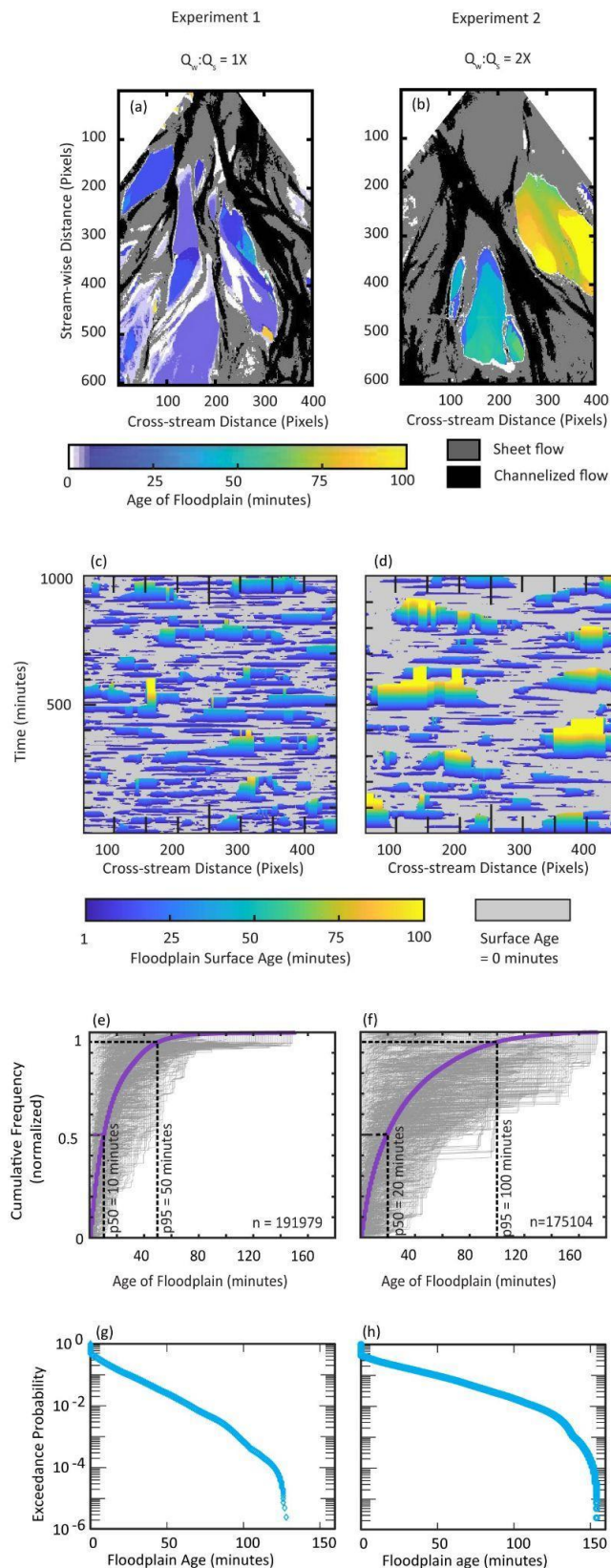


**Figure 4: Examples of floodplain ages mapped onto the dry areas of the experimental surface at one “snapshot” in time (1000 minutes) in Experiments 1 (a) and 2 (b). Time-space matrices showing floodplain surfaces and their age, encountered at any given time-step at a cross-stream transect in Experiments 1 (c) and 2 (d). Normalized cumulative frequency distributions of the ages of all floodplains encountered at the surface at each time-step (pale grey) and at all timesteps (bold magenta) along the same transect in Experiments 1 (e) and 2 (f), respectively. Exceedance probabilities associated with floodplains of different ages in Experiments 1 (g) and 2 (h).**